Exp Fluids (2012) 53:293–299
DOI 10.1007/s00348-012-1317-1

LETTER

Three-dimensional measurements of vortex breakdown

D. E. Calderon · Z. Wang · I. Gursul

Received: 30 November 2011 / Revised: 2 April 2012 / Accepted: 4 May 2012 / Published online: 22 May 2012

Abstract Leading-edge vortex formation and breakdown have been measured over a periodically plunging non-slender delta wing at a high angle of attack, using a three-dimensional particle-tracking method. A very rare type of vortex breakdown in the form of a double helix has been captured in the phase-averaged flow at a specific phase of the oscillation cycle.

1 Introduction

Vortex breakdown is a sudden expansion of vortices, which was first observed over delta wings. Related experimental investigations also included vortex breakdown generated in tubes. This has subsequently been investigated in detail, as this phenomenon affects both steady and unsteady aerodynamics of delta wings. Aspects of vortex breakdown over delta wings and tubes were reviewed by Hall (1972), Leibovich (1984), Escudier (1988), Rockwell (1993), Délery (1994) and Gursul (2005). Different explanations of this phenomenon were put forward over several decades.

Basically, 2 types of breakdown were identified, a bubble type and spiral type. The former appeared axisymmetric, whilst the latter appeared strongly non-axisymmetric with a spiral or corkscrew shape. Both types of breakdown were observed over delta wings and vortex tubes, although the spiral type is more common over delta wings (Gursul 2005).

The flow upstream of breakdown was found to be stable and perturbations to the vortex do not grow. However, the flow downstream of breakdown was found to be unstable and contained non-axisymmetric disturbances with periodic oscillations (Garg and Leibovich 1979; Gursul 1994). The disturbances may be presented as $\exp\{i(kx + n\phi - \omega t)\}$, where ω is the frequency, k the wavenumber in the axial direction, and n the wavenumber in the angular direction. It was shown that the periodic oscillations downstream of breakdown correspond to $|n| = 1$. This is consistent with the observations of the spiral breakdown. The bubble type is very rare over delta wings, and it was suggested that the spiral form is a consequence of the instability of the essentially axisymmetric (bubble-like) form (Escudier 1988). The axisymmetric type is generally found in axisymmetric geometries (tubes).

Higher modes ($|n| > 1$) are theoretically possible and may have increasing growth rate with increasing $|n|$ (Lessen et al. 1974). However, these higher modes are very rare experimentally. Instead, $|n| = 1$ mode is commonly found, which is the only mode having non-zero radial velocity component on the axis (Leibovich 1984). The boundary condition at the vortex axis requires finite and bounded velocity components. This condition requires that the amplitude of the azimuthal and radial velocity components must vanish at the vortex axis for all $|n| \neq 1$, this may explain why $|n| = 1$ mode is preferred experimentally as it is difficult to eliminate disturbances.

Only rare observations of a higher mode with $|n| = 2$ were made by Sarpkaya (1971) and Escudier and Zehnder (1982) in vortex tube experiments. Sarpkaya reported that extreme care for axisymmetry was essential in obtaining the $|n| = 2$ double helix mode. (The vortex was perfectly centred, and every precaution was taken to eliminate any disturbances). This mode was found highly sensitive to small disturbances, explaining why it is so rare to observe. To the best knowledge of the authors, the double helix mode was not previously observed over delta wings. This can be

D. E. Calderon · Z. Wang · I. Gursul (✉)
University of Bath, Bath BA2 7AY, UK
e-mail: i.a.gursul@bath.ac.uk

attributed to the lack of symmetry and possibly added disturbances due to the small-scale vortices that exist in the shear layer that wraps around the leading-edge vortex.

In this study, we show for the first time that the double helix mode exists over a plunging delta wing during some part of the oscillation cycle; it is repeatable and can be found in the phase-averaged flow field. This is accomplished by the application of a three-dimensional (3D) particle-tracking method for the three components of the velocity vector field in a volume.

2 Experimental methods

Experiments were carried out in a free-surface closed-loop water tunnel (Eidetics® Model 1520) at the University of Bath. It has a working test section that is 381 mm deep, 508 mm wide and 1,520 mm long. A speed controller allows variable flow speeds of up to 0.5 ms^{-1}. The flow is conditioned by a series of interchangeable elements, located upstream from the contraction section, in order to reduce turbulence intensity to less than 0.5 %.

The forced plunging motion is provided by a 'shaker mechanism', consisting of an AC 0.37 kW Motovario three-phase motor, using a 5:1 gearbox reduction and a basic rotary to linear crank mechanism. The crank arm was long enough to allow the wing to perform a near sinusoidal displacement. The maximum difference between a sinusoidal displacement and the theoretical displacement achieved by the crank mechanism is 0.75 % of the peak-to-peak amplitude. In order to verify this prediction, a PIV camera was used to track the trailing edge of the wing. The trailing-edge location was within 1.25 % of the sine curve. Conforming to a pure plunging motion, the angle of attack is fixed throughout the cycle. The frequency is managed by an IMO Jaguar Controller, and the amplitude is set by fixing the link bar at various distances from the centre of rotation. An illustration of the rig has been provided in Fig. 1.

Experiments were carried out on a delta wing with a sweep angle of $\Lambda = 50°$. This sweep angle was chosen because of the large amount of available data in the literature (Gursul et al. 2005). The wing was made from stainless steel, has a bevelled leading edge of 45° and round trailing edge. It has a root chord length of $c = 100$ mm, span of $b = 83.9$ mm and thickness of $t = 3$ mm. The wing design represents a half-span model that sits fully submersed in water, for which an endplate is used at the root to simulate the location of a symmetry plane. Clearance between the splitter plate and the wing was maintained at 1 mm, providing a gap of 1.0 %c. The blockage ratio achieved by the stationary wing is less than 1.0 % at 27° angle of attack. The latter was chosen based on the previous work (Gursul et al. 2005), in order to operate within a post-stall regime, consistent with vortex breakdown at the wing apex as well as fully separated flow over the wing. Force measurements and dye flow visualisation were carried out to confirm all the above.

The flow speed ($U_\infty = 0.214$ ms^{-1}) was adjusted to operate at a Reynolds number of 20,000 based on the root chord length. The enforced oscillatory plunging motion had an amplitude of $h = 0.15c$ and operated at a non-dimensional frequency of $St_c = fc/U_\infty = 0.4$, corresponding to a reduced frequency of $k = \pi fc/U_\infty = 1.26$. The maximum plunge velocity was 0.081 ms^{-1} (38 % of the freestream velocity), which corresponds to a change of effective incidence of 20.7°. Hence, the minimum and maximum angles of attack were 6.3° and 47.7° respectively.

The flow measurements presented in this study were acquired using a volumetric three-component velocimetry (TSI V3 V) laser system based on the techniques developed by Pereira and Gharib (2002) on defocusing digital particle image velocimetry (DDPIV). The volume of interest was illuminated using a dual ND:YAG 200 mJ pulsed laser, equipped with 2 cylindrical lenses placed at 90 degrees to each other to generate the required laser cone. Seeding was carried out using 50-μm hollow glass particles. The defocusing concept exploits the ability to use multiple off-axis apertures to generate defocused particle images whose separation distance and location can give an indication of the particles' position in 3D space. Three 4 MPixel 12 bit CCD cameras are placed to form an equilateral triangle. The intersection of their viewing cones produces an observable domain whose most distant point is set as the intersection of the 3 focal planes. If the 3 images were superimposed, a particle in 3D space would appear thrice on the vertices of a triangle, corresponding to each of the 3 cameras. The centre and size of the triangle determines the particle's in-plane and out-of-plane location, respectively.

A rectangular plate with 5-mm spaced grid dots is translated across the volume of interest, capturing an image at 5 mm intervals, which are then filtered through a particle identification algorithm in order to calibrate the system and generate a camera signature graph. Experiments were carried out using a pair of laser cones, fired 900 μs apart, straddling 2 neighbouring camera frames. The particles are identified in each of the 6 captured images using 2D Gaussian fitting. Three-dimensional coordinates are then determined using triangulation of the particle images based on the calibration triplets for each set of captured images. A 3D particle-tracking algorithm, first proposed by Baek and Lee (1996), is performed based on the triplets identified in each of these camera frames. The relaxation method essentially uses an iterative process to update the probability of 2 particles matching between 2 frames, at each step, using neighbour particle displacement similarity criteria as well as flow estimates, and then choosing the

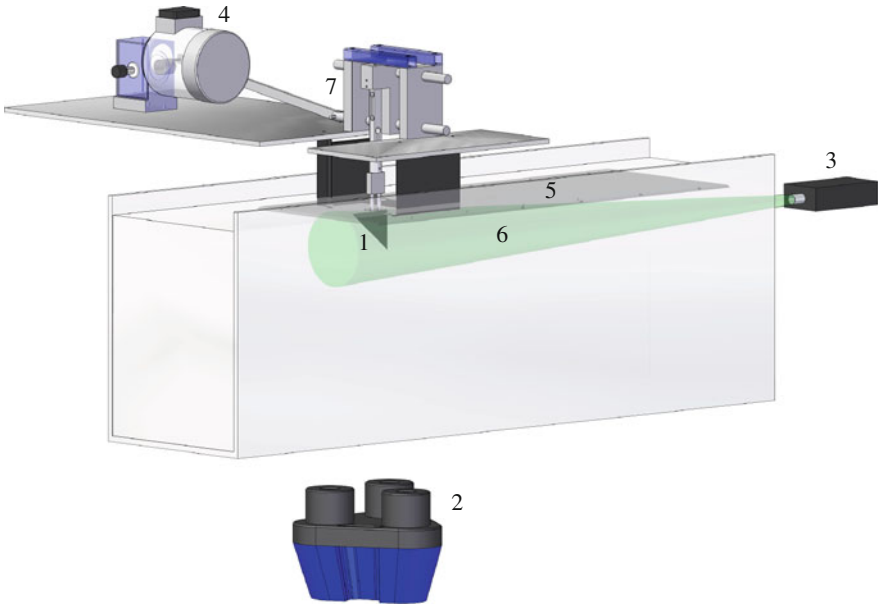

Fig. 1 Experimental set-up. *1* Delta wing, *2* Camera, *3* Laser unit, *4* Motor, *5* End plate, *6* Laser volume, *7* Shaker mechanism

particle match with greatest probability. This is outlined in more detail by Pereira et al. (2006). In addition, a median filter was applied to remove any outliers. The final step uses Gaussian interpolation on the randomly spaced vectors to generate a series of uniformly spaced velocity vectors centred within 8 mm voxels with 65 % overlap, producing a spatial resolution of 2.8 %c. These instantaneous velocity vectors have a combined uncertainty of less than 3 %.

A rotary encoder was fitted to the worm gear that generated 360 pulses per cycle. This was used to trigger the Laser Pulse synchroniser and thus fire the laser repeatedly at any desired phase in the plunging motion. The velocity vectors presented in the current study are all computed based on phase averaging 140 vector fields. The grid interpolation ultimately produced around 80,000 grid vectors within a measurement volume of 165.2 × 156.8 × 98.0 mm. The size and relative position of the measurement volume, with respect to the wing and its motion, is illustrated in Fig. 2. The calibration procedure near the end plate resulted in a loss of 3 mm at the root of this half model wing. Note that a small portion of the leading-edge vortex is not captured near the apex because of this reason.

Velocity vector fields were processed within Matlab, in order to compute the desired flow properties. These were then passed over to Tecplot 360 for final analysis. Isosurfaces were developed, predominantly based on vorticity magnitude. However, in order to distinguish between vortical structures and shear flows, an additional vortex detection algorithm, the Q-criterion, has been put to use. Hunt et al. (1988) first suggested that a vortex can be characterised based on the second invariant of the deformation tensor. The criterion is based on the ability to decompose the deformation tensor ∇u into symmetrical

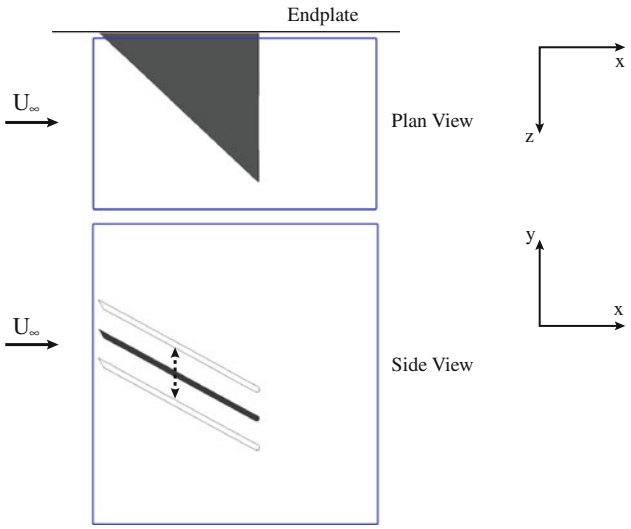

Fig. 2 Measurement volumes

and antisymmetrical parts, $S = 0.5(\nabla u + \nabla u^T)$ and $\Omega = 0.5(\nabla u - \nabla u^T)$ (T is the transpose), defining the rate of strain and vorticity tensors, respectively. If $Q = 0.5\left(||\Omega||_E^2 - ||S||_E^2\right) > 0$, such that $||\cdot||_E$ represents the Euclidean norm, rotational effects dominate and a vortex is said to be identified. Further details on the 'Q-Criterion' can be found in Jeong and Hussain (1995).

3 Results

Volumetric velocimetry measurements were acquired at four phases in the cycle and are presented in Fig. 3. In

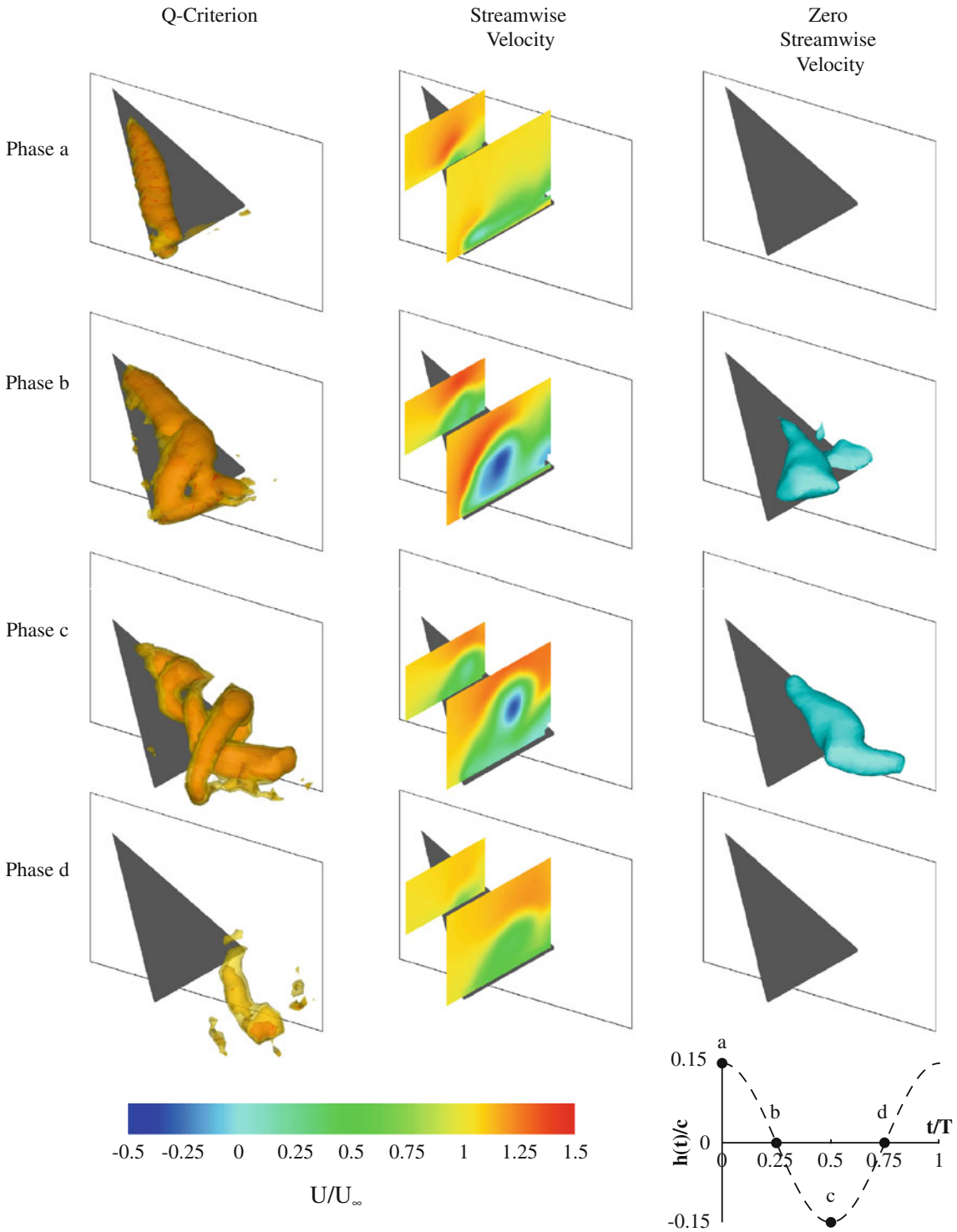

Fig. 3 From *left* to *right*: an isometric view of Q-criterion ($Qc/U_\infty = 23.5$, 28 and 42) iso-surfaces, cross-stream slices showing streamwise velocity and zero streamwise velocity iso-surfaces, at 4 phases in the plunging cycle

the left column, iso-surfaces are defined by positive Q-criterion in order to exclude localised regions in which shear effects dominate over rotational flow. Values of the streamwise velocity component at 2 separate cross-stream planes have also been presented together with an iso-surface representation of the zero streamwise velocity. The phases correspond to the vertical extremities and centreline of the plunging motion. The rectangular region sketched at the root of the wing represents the endplate, or symmetry plane.

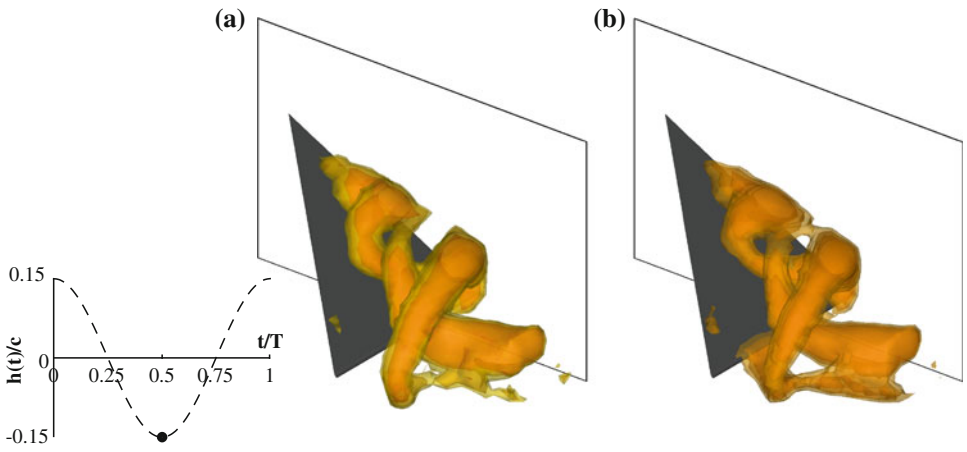

Fig. 4 An isometric view of **a** the Q-criterion ($Qc/U_\infty = 23.5$, 28 and 42) and **b** vorticity magnitude ($|\omega|c/U_\infty = 10$, 11 and 12) iso-surfaces at the *bottom* of the plunging motion

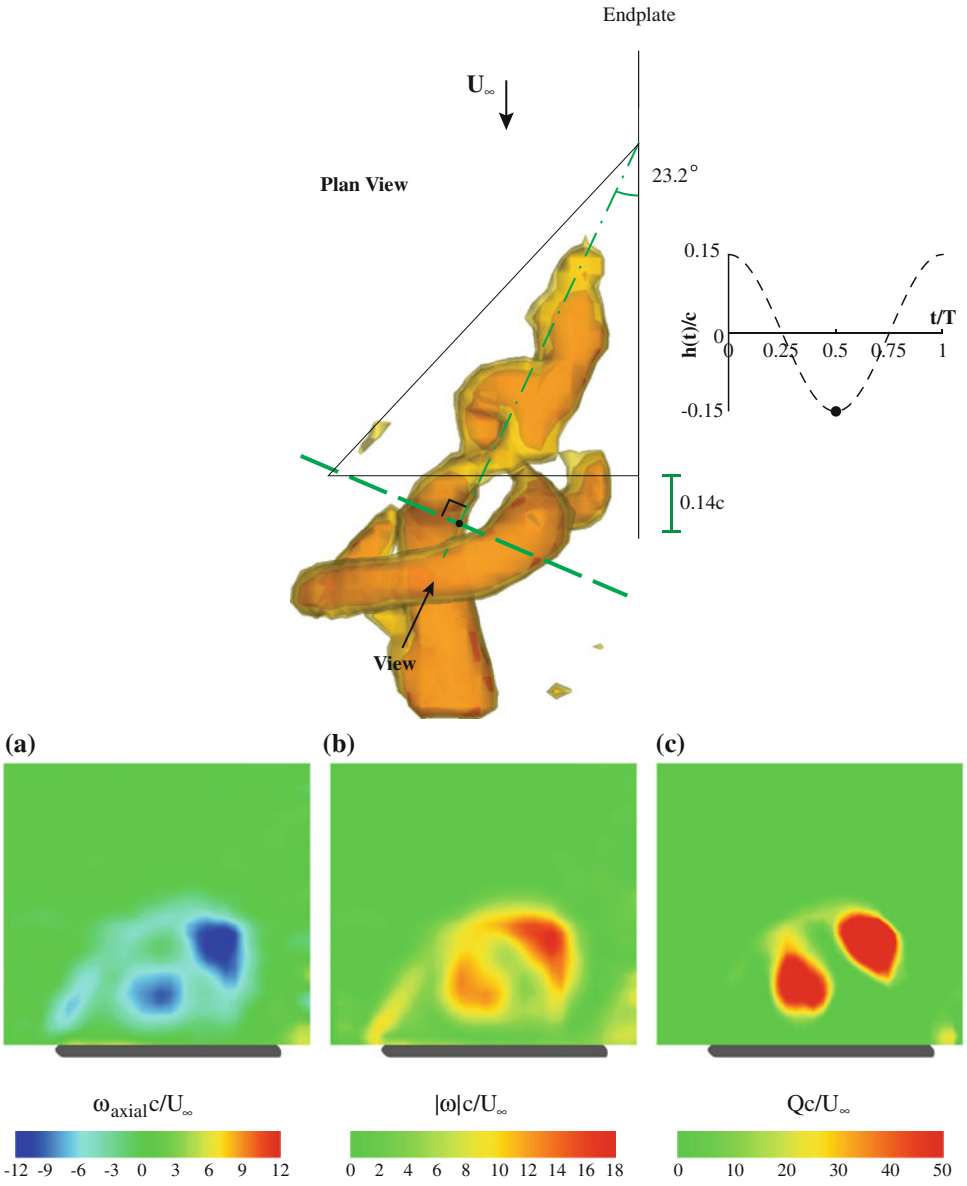

Fig. 5 A comparison between **a** non-dimensionalised axial vorticity, **b** vorticity magnitude and **c** positive Q-Criterion at a *plane* near the trailing edge of the wing specified by the *dashed line*

Despite the high geometric angle of attack, a coherent leading-edge vortex structure is present at $t/T = 0$, the top of the oscillation. At this point in the cycle, the effective angle of attack, induced by the plunging motion, is equivalent to the geometric angle of attack, after having passed a minimum at phase d. The leading-edge vortex forms close to the surface of the wing, in a similar manner to stationary wings at low angles of attack. Despite the formation of a coherent leading-edge vortex at the top of the oscillation, there appears to exist no axial jet-like profile. For stationary wings, it is not uncommon to observe axial velocity profiles with no excess velocity, or even broad wake-like velocity, at the low angles of attack and Reynolds numbers (Gursul et al. 2005). This is in contrast to the observations for the leading-edge vortices over slender delta wings.

As the wing progresses through the plunging motion reaching maximum plunge velocity at $t/T = 0.25$, the centre of the vortex begins to move inboard and away from the wing. It is interesting to see that this is consistent with the relationship between vortex location and increasing angle of attack of a stationary non-slender delta wing. Reversal of the mean axial velocity is now observed near the trailing edge, which is an indication of vortex breakdown. The onset of breakdown is not abrupt, with the core expanding in a conical fashion, as is typically seen in non-slender delta wings. We also observe the concurrent formation of a trailing-edge vortex, which in agreement with Helmholtz's Second theorem, remains connected to the leading-edge vortex, resulting in the deformation of the leading-edge vortex structure.

At $t/T = 0.5$, we observe the presence of a double helix structure with a sense of rotation opposite to that of the 2 vortex filaments. The structure represents a form of vortex breakdown that has not been reported before over a delta wing. Moreover, the measurements are phase-averaged, which indicates an adequate level of repeatability of this structure between cycles. [Maximum standard deviation of the phase-averaged velocity magnitude has been found to be about 30 % of the freestream velocity near the vortex axis. Although this appears to be large, it is typical for the vortex meandering over delta wings (Gursul, 2005)]. Slices at different chordwise locations indicate the presence of flow reversal at the centre of the structure, enclosed by a region of zero streamwise velocity (see Phase c, middle column in Fig. 3). Interestingly, the iso-surface of zero velocity exhibits a clear undulation (see Phase c, right column in Fig. 3). Remnants of the helix structure are observed downstream of the wing halfway through the upstroke.

Figure 4 compares the effect of using non-dimensional vorticity magnitude to define iso-surfaces at the bottom of the oscillation ($t/T = 0.5$). Similarities between the 2 defining parameters (Q-criterion and vorticity magnitude) are evident. Various parameters are shown at a plane near the trailing edge of the wing and normal to the vortex axis in Fig. 5. This plane is shown by the dashed line in the figure and its intersection with the vortex axis is located 0.14 c from the trailing edge as also sketched in the same figure. The double helix structure is better represented in this plane with all 3 variables (axial vorticity, total vorticity magnitude and Q-criterion), while the Q-criterion provides the clearest view.

4 Conclusions

A double helix structure has been observed over a non-slender delta wing with a sweep angle of 50° undergoing a small amplitude plunging motion with fixed geometric angle of attack of $\alpha = 27°$ in the post-stall region. A region of reverse axial flow resides at the centre of this structure, which occurs at the bottom of the oscillation. Various parameters have been used to analyse the flow. A vortex identification algorithm, the Q-criterion, has been shown to improve the visualisation of this structure.

The $|n| = 2$ mode of breakdown is highly sensitive to external disturbances and rare in the vortex tube experiments and has never been observed over stationary delta wings. We show in this study that the double helix mode exists over a plunging non-slender delta wing. It is highly repeatable and appears in the phase-averaged flow. This study is also the first to perform volumetric measurements of vortex breakdown using a 3D particle-tracking method. Without this volumetric measurement technique, the reported vortex breakdown structure would be very difficult to capture.

Acknowledgments This work was sponsored by the Air Force Office of Scientific Research, Air Force Material Command, USAF under grant number FA8655-10-1-3093, monitored by Dr. D. Smith, as well as the Engineering and Physical Sciences Research Council (EPSRC) Studentship.

References

Baek SJ, Lee SJA (1996) New two-frame particle tracking algorithm using match probability. Exp Fluids 22:23–32

Délery JM (1994) Aspects of vortex breakdown. Prog Aerosp Sci 30:1–59

Escudier MP (1988) Vortex breakdown: observations and explanations. Prog Aerosp Sci 25:189–229

Escudier MP, Zehnder N (1982) Vortex-flow regimes. J Fluid Mech 115:105–121

Garg AK, Leibovich S (1979) Spectral characteristics of vortex breakdown flowfields. Phys Fluids 22:2053–2064

Gursul I (1994) Unsteady flow phenomenon over delta wings at high angle of attack. AIAA J 32:225–231

Gursul I (2005) Review of unsteady vortex flows over slender delta wings. J Aircr 42:299–319

Gursul I, Gordnier R, Visbal M (2005) Unsteady aerodynamics of nonslender delta wings. Prog Aerosp Sci 41(7):515–557

Hall MG (1972) Vortex breakdown. Annu Rev Fluid Mech 4:195–218

Hunt JCR, Wray AA, Moin P (1988) Eddies, stream, and convergence zones in turbulent flows. In: Center for turbulence research report. Center for Turbulence Research, Stanford, USA, pp 193–208

Jeong J, Hussain F (1995) On the identification of a vortex. J Fluid Mech 285:69–94

Leibovich S (1984) Vortex stability and breakdown: survey and extension. AIAA J 22:1192–1206

Lessen M, Sing PJ, Paillet F (1974) The stability of a trailing line vortex. Part 1. Inviscid theory. J Fluid Mech 63:753–763

Pereira F, Gharib M (2002) Defocusing digital particle image velocimetry and the three-dimensional characterization of two-phase flows. Meas Sci Technol 13:683–694

Pereira F, Stuer H, Graff EC, Gharib M (2006) Two-frame 3D particle tracking. Meas Sci Technol 17:1680–1692

Rockwell D (1993) Three-dimensional flow structure on delta wings at high angle of attack: experimental concepts and issues, AIAA paper 93-0550

Sarpkaya T (1971) On stationary and travelling vortex breakdowns. J Fluid Mech 45:545–559